Nuclear Instruments and Methods in Physics Research B 325 (2014) 107–114

Contents lists available at ScienceDirect

Nuclear Instruments and Methods in Physics Research B

journal homepage: www.elsevier.com/locate/nimb

Electrical properties of deuteron irradiated high resistivity silicon

Jerzy Krupka [a,*], Waldemar Karcz [b,c], Sergej P. Avdeyev [c], Paweł Kamiński [d], Roman Kozłowski [d]

[a] Insitute of Microelectronics and Optoelectronics, Warsaw University of Technology, Koszykowa 75, 00-662 Warsaw, Poland
[b] H. Niewodniczański Institute of Nuclear Physics Polish Academy of Science, Cracow, Poland
[c] Joint Institute for Nuclear Research, Joliot-Curie 6, 141980 Dubna, Russia
[d] Institute of Electronic Materials Technology, Wólczyńska 133, 01-919 Warsaw, Poland

ARTICLE INFO

Article history:
Received 18 October 2013
Received in revised form 17 January 2014
Available online 14 February 2014

Keywords:
Silicon detector
Resistivity
Radiation damage
Defects
HRPITS

ABSTRACT

We have investigated resistivity changes introduced on the high-resistivity *p*-type silicon wafer by the irradiation with deuteron beam with an energy of 4.4 GeV performed in the NUCLOTRON superconducting accelerator. Two contactless techniques were used for the measurements of resistivity changes: namely the microwave split post dielectric resonator (SPDR) technique and capacitance measurements in the frequency domain. The first technique allows resistivity measurements in the plane of the wafer, while the second one in the direction perpendicular to the wafer. The resistivity map obtained with the SPDR technique enabled us to obtain a permanent fingerprint of the accelerator beam intensity profile. It has been shown that after the irradiation, the material resistivity increased to $\sim 3.9 \times 10^5\ \Omega$ cm in the wafer region exposed to the maximum beam intensity. Complementary studies of the properties and concentrations of radiation deep-level defects were performed by the high-resolution photo-induced current transient spectroscopy (HRPITS). These studies have shown that the irradiation of the high resistivity silicon with 4.4-GeV deuterons results in the formation of several types of deep-level defects responsible for the charge compensation.

1. Introduction

High-resistivity silicon detectors are commonly used in nuclear accelerators including the Large Hadron Collider at CERN. It is already well known that electrical properties of silicon subjected to irradiation with high-energy particles significantly deteriorate due to a damage of the crystal lattice [1–2]. Studies of the radiation damage have been undertaken by many researchers and a number of various experimental techniques have been employed for this purpose [3–8]. To investigate evolution of the electrical properties of silicon after irradiation, the results of Hall effect measurements have been used [9–10] as well as theoretical calculations of defect levels have been made [11,12]. An interesting experimental technique is the pocket pumping method [13]. In this method [13], a Charge-Coupled Device (CCD) is illuminated with a low light intensity to obtain a flat field level and then the accumulated charge of a number of pixels is shifted back and forth in the parallel direction. After doing this for a certain fixed number of cycles, the CCD is read out in the normal manner. Numerous studies of irradiation-induced defects in Si have been also carried out by other techniques like deep level transient spectroscopy (DLTS), electron paramagnetic resonance (EPR), photoluminescence spectroscopy (PL), Fourier transform infrared absorption (FTIR). The properties of radiation defect centers determined from these studies are reported in the references [14–20].

In this work we investigate the resistivity changes in a high resistivity float zone (FZ) *p*-type silicon wafer (6 inch in diameter) introduced by the irradiation with a deuteron beam with the energy of 4.4 GeV. Two contactless techniques are used for the measurements of resistivity changes: namely microwave split post dielectric resonator (SPDR) technique and capacitance measurements in the frequency domain. [21]. The first technique enables resistivity measurements in the plane of the wafer, while the second one in the direction perpendicular to the wafer. The resistivity map obtained by means of the SPDR technique allows obtaining a permanent fingerprint of the accelerator beam intensity profile. Complementary studies of the properties and concentrations of radiation deep-level defects are performed by the high-resolution photo-induced current transient spectroscopy (HRPITS). Using the HRPITS results, a charge compensation model for the irradiated material is proposed.

* Corresponding author. Tel.: +48 501237390.
E-mail address: krupka@imio.pw.edu.pl (J. Krupka).

http://dx.doi.org/10.1016/j.nimb.2014.01.021
0168-583X/

2. Resistivity studies

In our experiment we have used a high resistivity (HR) *p*-type FZ silicon wafer with a diameter of 152 mm and thickness of 990 μm manufactured by TOPSIL. At first, the resistivity map on the virgin wafer was measured with a split post dielectric resonator scanner operating at a frequency of ~5 GHz. Then the wafer was sent to the Joint Institute for Nuclear Research, Laboratory of High Energy Physics (Dubna, Russian Federation). The irradiation of the wafer has been performed at the external beam of the Dubna superconducting accelerator called NUCLOTRON. The Nuclotron is a basic facility of the Laboratory of High Energy Physics at the Joint Institute for Nuclear Research aimed at obtaining beams of multicharged ions (nuclei) with the energy up to 6 GeV per nucleon, from proton to Bi beams, as well as producing polarized deuteron beams. The beam spot was continuously controlled by two multiwire proportional chambers. The beam intensity was measured using the ionization chamber. For deuterons, the beam intensity was around 10^8 particles per spill. The spill length was 1.5 s, the frequency of the beam bursts was 0.1 Hz. Our Si wafer was irradiated with the 4.4-GeV deuterons at the intensity of 6.12×10^8 deuterons/cm^2/s. The integral intensity was 1.61×10^{14} cm^{-2}. The intensity was measured off line by the Al foil irradiation together with the wafer and the registration of gamma radiation with an energy of 1368 and 2754 keV from the ^{24}Na source (resultant reaction ^{27}Al(d,3p2n)^{24}Na).

The resistivity measurements on the silicon wafer have been performed employing the split post dielectric resonator operating at a frequency of 5 GHz and independently employing an Agilent Technologies 16451B capacitive dielectric test fixture that are presented in Fig. 1. Using SPDR, the real and the imaginary part of the material permittivity are determined and then the resistivity is calculated from the imaginary part of permittivity. For the measurements using the capacitive cell, a four layer model (air gap above the sample, bulk silicon and two depletion layers) is assumed. Parameters of such a model are determined from the broad-range frequency measurements of the effective capacitance and the Q-factor of the cell containing the wafer under test. The frequency corresponding to the last Q-factor minimum is inversely proportional to the resistivity of the bulk silicon layer. More details about the two measurement techniques can be found elsewhere [22]. It should be mentioned here that for the both techniques, the microwave and the RF current densities in the direction perpendicular to the high resistivity wafer were almost uniform. However for the microwave technique, the electric currents had only azimuthal component (in the plane of the wafer) while for RF technique, the electric currents were perpendicular to the wafer.

The maps of the resistivity component parallel to the wafer surface before and after irradiation, obtained from the measurements by means of the SPDR scanner, are presented in Figs. 2 and 3. One can observe that the resistivity of the virgin (not irradiated) material exhibits variation in the range from 144 to 210 Ω m. After the irradiation, the resistivity significantly (more than 15 times) increases and its distribution around the point where the deuteron beam was focused reassembles spatial distribution of the beam intensity. This is clearly visible in Fig. 3b. Using the SPDR method, the resistivity values were calculated neglecting dielectric losses. The maximum resistivity value of 2690 Ω m obtained using the

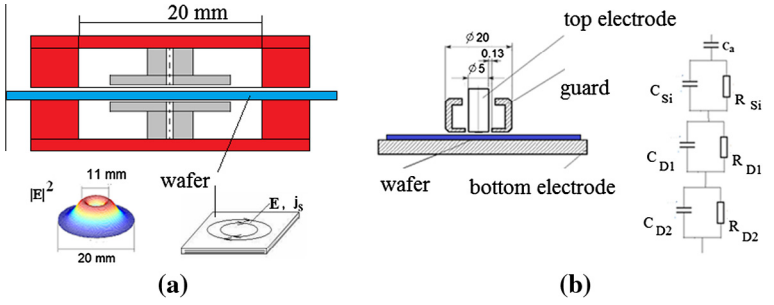

Fig. 1. (a) Sketch of the split post dielectric resonator (SPDR). Pictures below the SPDR show the electric field (electric current) lines in the sample and spatial distribution of the electric field energy. (b) Capacitive cell and its equivalent circuit model for a HR silicon sample.

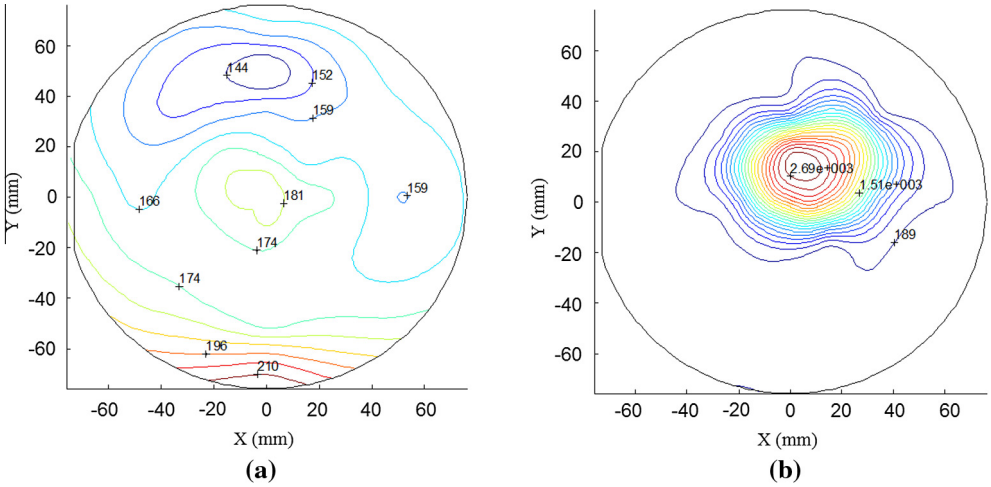

Fig. 2. In-plane resistivity map of *p*-type silicon wafer obtained with the SPDR scanner operating at a frequency about 5 GHz (a) before irradiation and (b) after irradiation. Resistivity unit (Ω m).

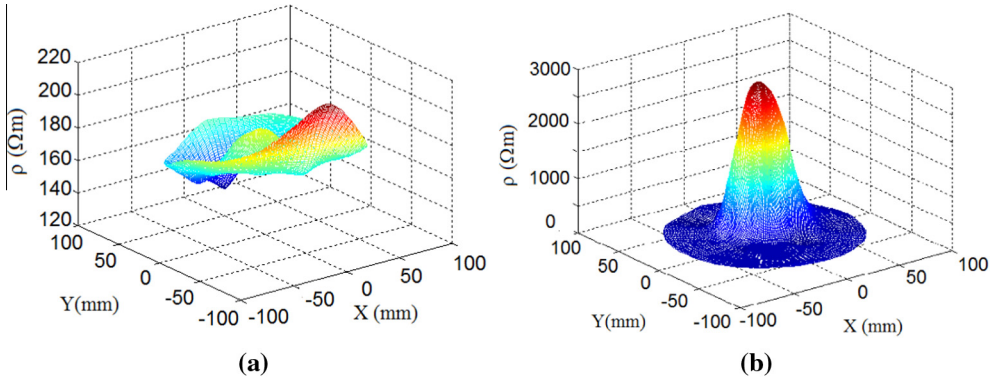

Fig. 3. 3D in-plane resistivity map of the *p*-type silicon wafer obtained with the SPDR scanner operating at a frequency about 5 GHz (a) before irradiation and (b) after irradiation.

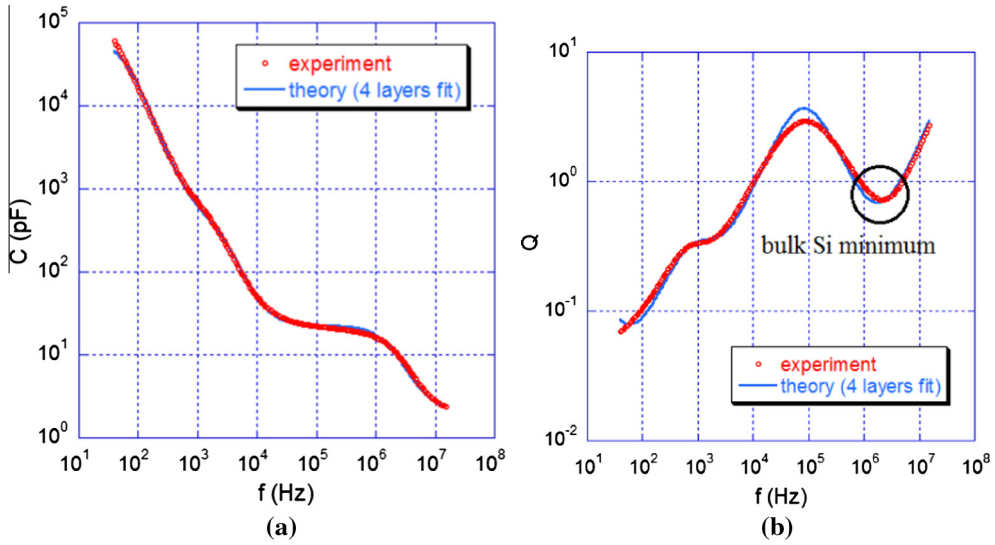

Fig. 4. Capacitance and Q-factor measured at the point at the edge of the irradiated silicon wafer. The point coordinates are: $X = 0$ mm, $Y = -65$ mm. Fitting parameters: $h_a = 2.7$ nm, $h_{D1} = 92.9$ μm, $\rho_{D1} = 1.31 \times 10^7$ Ω cm, $h_{D2} = 3.89$ μm, $\rho_{D2} = 2.28 \times 10^8$ Ω cm, $\rho_{Si} = 2.63 \times 10^4$ Ω cm.

SPDR method corresponds to the total dielectric loss tangent of 8.5×10^{-5}. This is slightly above the upper resistivity measurement limit for the SPDR technique. At this low loss level, the dielectric losses probably constitute a significant part so in reality, the maximum resistivity of the irradiated wafer is larger than 2690 Ω m.

It should be mentioned that together with the measurements of the imaginary part of permittivity we also measured the real part of permittivity. Its value proved to be constant within the limits of measurement uncertainties at every data point on the wafer measured before and after irradiation. The real part of the permittivity value as measured by means of the SPDR is equal to 11.65 (+/−) 0.5%. The capacitance measurements have been performed at two distinct points of the irradiated wafer. The first of the points with point coordinates $X = 0$ mm, $Y = -65$ mm was situated at the edge of the irradiated silicon wafer. The second point with coordinates $X = 7$ mm, $Y = 10$ mm was situated at the maximum beam intensity. The results of these measurements are shown in Figs. 4 and 5. The main difference between results for the two points is manifested by a significant change in the frequency where the last Q-factor minimum on the frequency axis appears. One can see that the frequency of the last minimum is about 2.5 MHz at the data point for the not irradiated wafer region, while it is about 140 kHz at the point for the irradiated region corresponding to the maximum beam intensity. The best fit to the measurement data have been obtained by the optimization procedure involving the frequency minimum search on the MATLAB platform for the sets of parameters. The values of these parameters are shown in Table 1.

It should be noted that resistivity values for the bulk silicon layer measured in the direction perpendicular to the wafer agree very well with those measured by means of the SPDR scanner at the same points in the direction in the plane of the wafer. This means that the resistivity can be considered as isotropic quantity in the bulk silicon layer for both the virgin and irradiated regions of the wafer.

Presence of depletion layers for the virgin and irradiated regions is related to the presence of surface state charges on the silicon wafer surface. It should be noted that for high resistivity silicon even small concentration of the surface state charges induces deep depletion layer. It is well known phenomenon and it is enhanced when the sample is processed at high temperatures (e.g. high temperature oxidation). A larger concentration of surface state charges would even lead to the appearance of inversion layer (electron gas) in the vicinity of the silicon wafer surface [22]. Comparing the resistivity of depletion layers for the non-irradiated and heavily irradiated regions, one can conclude that there is the change due to irradiation-induced deep-level defects. The resistivity of the

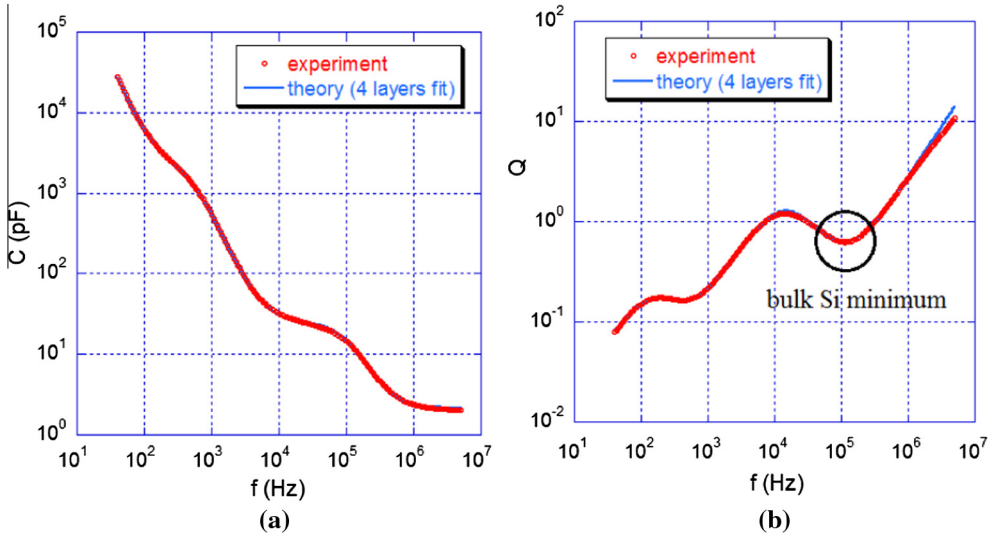

Fig. 5. Capacitance and Q-factor measured at the point of maximum beam intensity for the irradiated silicon wafer. The point coordinates are: $X = 7$ mm, $Y = 10$ mm. Fitting parameters: $h_a = 0.5$ nm, $h_{D1} = 83.8$ μm, $\rho_{D1} = 3.02 \times 10^7$ Ω cm, $h_{D2} = 0.816$ μm, $\rho_{D2} = 1.17 \times 10^9$ Ω cm, $\rho_{Si} = 3.94 \times 10^5$ Ω cm.

Table 1
Parameters of multilayered model of silicon sample evaluated by the optimization procedure as the best fit to the measurement data.

Parameter	Edge point	Maximum beam intensity point
ρ_{Si} (Ω cm)	2.63×10^4	3.94×10^5
h_{Si} (μm)	893.2	905.4
ρ_{D1} (Ω cm)	1.31×10^7	3.02×10^7
h_{D1} (μm)	92.9	83.8
ρ_{D2} (Ω cm)	2.28×10^8	1.17×10^9
h_{D2} (μm)	3.89	0.82
h_a (nm)	2.7	0.5

dominant part of the depletion layer has increased from 1.31×10^7 Ω cm for the virgin region to 3.02×10^7 Ω cm for the irradiated region. However the depth of depletion layers remained similar for virgin and irradiated samples so we postulate that the concentrations of the surface state charges remained similar before and after the irradiation.

3. HRPITS studies of radiation deep-level defects

The properties and concentrations of radiation defect centers were determined by the high-resolution photoinduced transient spectroscopy (HRPITS) using an intelligent measuring system described elsewhere [23]. Samples with dimensions of 4×7 mm^2 were cut from the wafer at the various distance from the region irradiated with the dose corresponding to the maximum deuteron beam intensity. We have used three samples, labeled as A, B and C, of the wafer regions located at the distance of 2, 10 and 18 mm from the region irradiated with the maximum of the deuteron beam intensity, respectively. On each sample, two co-planar ohmic contacts were made by evaporating a 300-nm layer of Al through a metal mask. The contacts were in the shape of squares with the area of 2.1×2.1 mm^2 and the gap between them was 0.7 mm.

Before the HRPITS measurements, the temperature dependences of dark current (TDDC) were determined. For the A and B samples, these dependences are exemplified in Fig. 6. The dependences can be qualitatively explained by assuming that the charge carrier compensation results from the balance between the oxygen-related irradiation-induced shallow donors and deep acceptors related to vacancy aggregates. This assumption is fully justified for

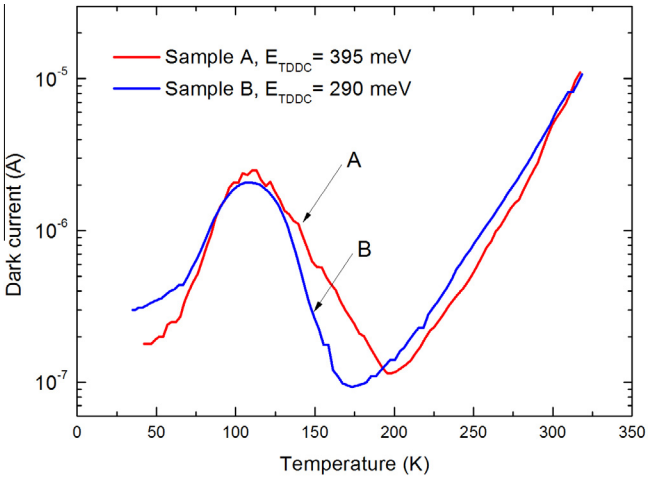

Fig. 6. Temperature dependences of dark current for two samples of deuteron irradiated FZ Si labeled as A and B. The samples are of the wafer regions located at the distance of 2 and 10 mm from the region irradiated with the maximum intensity of deuteron beam, respectively. E_{TDDC} is the activation energy of dark conductivity determined at the temperature range of 270–310 K.

silicon irradiated with high doses of hadrons [12,24]. The shallow donors, tentatively identified as oxygen-related irradiation-induced shallow donors, were observed earlier in Si grown either by the FZ or Czochralski (Cz) technique, as well as in epitaxial silicon subjected to irradiation with high fluences of high-energy neutrons or protons [23,25,26]. The activation energy of these centers determined from the HRPITS studies ranges from 10 to 30 meV [23,26] and is in an agreement with the ionization energy of 26 meV obtained from the Hall measurements [25]. It was found that the concentration of the 10-meV centers produced by the 1-MeV proton bombardment with the fluence of $\sim 2 \times 10^{14}$ cm^{-2} is dependent on the oxygen concentration. In the Cz-Si, with the oxygen concentration of $\sim 5 \times 10^{17}$ cm^{-3}, the concentration of the 10-meV centers was $\sim 2 \times 10^{13}$ cm^{-3}, whereas in the FZ-Si, with the oxygen concentration of $\sim 10^{16}$ cm^{-3}, the concentration of these centers was by the order of magnitude lower. The irradiation-induced shallow donor centers are likely to be associated with electrically active small aggregates of oxygen atoms that can be

formed during irradiation even at room temperature [27–29]. This possibility is due to the radiation-enhanced diffusion of oxygen atoms that is particularly efficient when the material is irradiated with high doses of high-energy heavy particles. In other words, the diffusivity of oxygen is strongly dependent on the concentrations of irradiation-induced native point defects created in the material [28,29]. The well-known oxygen-related thermal donors that are formed in not irradiated Cz-Si by annealing at 450 °C are also identified with oxygen aggregates [30]. Because the native point defects concentrations in an as-grown Si single crystal are by orders of magnitudes lower compared to those in an irradiated material, a higher temperature is needed to make the diffusivity of oxygen atoms sufficient for the formation of these aggregates [28,29]. Furthermore, a high concentration of oxygen atoms is necessary. The thermal donors arising in 450 °C heat-treated oxygen-rich silicon were found to be double donors, with the energy levels at 60 and 130 meV below the conduction band edge corresponding to the changes of the charge state (0/+) and (+/++), respectively [31]. The difference in the electronic properties of the oxygen-related thermal donors occurring in the irradiated Si and in the as-grown heat treated material is likely to result from the different size of the oxygen aggregates and arrangement of the forming them oxygen atoms. These properties can also be affected by the different arrangement of silicon atoms in the vicinity of an oxygen atoms aggregate. [27].

The maximum of the dark current at the temperature around 100 K indicates that a metastable deep acceptor defect must be involved in the charge compensation. The metastability is considered to be an effect resulting from a large electron–phonon interaction causing a change in the atomic configuration of the defect associated with a change in its electronic structure [11,32]. The transition from the metastable state to the stable equilibrium defect state is thermally activated and for defects responsible for the dark current changes shown in Fig. 6 this transition is in the range of 100–200 K. In the metastable state at ~100 K these defects are fully neutral and the material becomes of *n*-type with a higher electron concentration and much higher electron mobility. Thus, the increase in the dark current at the range of 50–100 K is due to the rise in the electron concentration as a result of the ionization of the irradiation-induced donor centers. At the temperature ~100 K, the donor centers are fully ionized and the metastable deep acceptors are neutral. At the temperature of ~175 K for the B sample and ~200 K for the A sample, the deep acceptors are fully in the stable state, so they are negatively charged and the material is of *p*-type and highly compensated.

The increase of dark current in the temperature range of ~220–310 K is mainly due to the electron emission from the deep acceptors accompanied by an increasing rate of the thermal generation of the electron–hole pairs. The activation energies of dark conductivity in the temperature range of 270–310 K, estimated from the TDDC measurements for the A, B and C samples, are 395, 290 and 100 meV, respectively. It is worth adding that the resistivity of the A, B and C samples at 300 K is 2.7×10^5, 2.3×10^5 and $\sim 1.0 \times 10^5\ \Omega$ cm, respectively.

In the HRPITS method, the levels in the bandgap are filled with the excess charge carriers generated by optical pulses and the information about the traps properties is extracted from the photocurrent relaxation waveforms observed when the illumination is switched off. For the A, B and C samples, the measurements of photocurrent transients were carried out in the temperature range of 200–320 K with the increment of 2 K. The excess charge carriers were generated in the region between the two contacts by a semiconductor laser emitting the red light excitation pulses with the wavelength of 650 nm (1.91 eV). The power of the laser beam was 1.1 mW corresponding to the photon flux of 1.4×10^{17} cm^{-2} s^{-1}. The excitation pulse duration time and the repetition period were 10 and 500 ms, respectively. The voltage between two co-planar contacts was 10 V. The photocurrent transients were amplified using a Keithley 428 fast current amplifier (conductance-voltage converter) and then digitized with a 12-bit amplitude resolution and a 1-μs time resolution. In order to improve the signal to noise ratio the digital data were averaged taking 250 waveforms. For further processing, each photocurrent relaxation waveform was normalized with respect to the photocurrent amplitude at the end of the optical pulse. At 300 K, the Si absorption coefficient for the 1.91-eV photons is $\sim 4 \times 10^3$ cm^{-1}, which gives the light penetration depth of ~2.5 μm.

When retrapping of the excess charge carriers by the defect centers is neglected, the part with the time constant longer than ~1 μs of a photocurrent relaxation waveform is related to the thermal emission of charge carriers and the reciprocal of this time constant is equal to the emission rate [33]. The images of experimental spectral fringes are obtained by means of the two-dimensional analysis of the photocurrent relaxation waveforms using the correlation procedure and the numerical procedure based on the inverse Laplace transform algorithm (ILT) [33]. As a result, the temperature changes in the time constants of the relaxation waveforms are visualized in the 3D space as the spectral surface being a function of two variables: the temperature (T) and emission rate (e_T). The processes of thermal emission of charge carriers from detected defect levels are seen as the folds on the spectral surface, and the projections of these folds on the plane determined by the axes (T, e_T) give the experimental spectral fringes. It is worth noting that the resolution of the ILT procedure, involving fitting the photocurrent relaxation waveforms with multi-exponential functions by means of the CONTIN program [33], is much higher than that of the correlation procedure and enables closely spaced defect levels to be distinguished [33]. The projection of the ridgeline of each fold, occurring in the correlation or Laplace spectral surface, on the plane determined by the axes (T, e_T) gives the temperature dependence of the emission rate for the particular defect center [33]. For each trap detected, the projected line is fitted with the Arrhenius formula [33].

$$e_T(T) = AT^2 \exp(-E_a/k_B T), \tag{1}$$

where e_T is the thermal emission rate of electron and holes, T is the temperature, E_a is the activation energy, k_B is the Boltzmann constant and $A = \gamma\sigma$ is the product of the material constant γ and the apparent capture cross-section σ for electrons or holes. As a result, the activation energy E_a and the pre-exponential factor A, related to the capture cross-section, are calculated.

The trap concentration N_T is determined in two steps. First the concentration $n_T(0)$ of charge carriers trapped at the moment of switching off the optical pulse is calculated from the formula:

$$n_T(0) = \frac{I_0 S(T_{\max})}{q e_T BEC(\lambda, T)\mu\tau} \tag{2}$$

where q is the charge of an electron, I_0 is the photocurrent amplitude at the end of illumination pulse, $S(T_{\max})$ is the height of the fold $S(T_{\max})$ in the correlation spectrum, e_T is the thermal emission rate at the temperature $T_{\max}$, E is the applied electric field, and $\mu\tau$ is the product of the mobility and lifetime of charge carriers. The parameters B and $C(\lambda, T)$ are given below:

$$B = \exp(-e_T t_1) - \exp(-e_T t_2), \tag{3}$$

$$C(\lambda, T) = \left(\frac{1}{\alpha} + L_D\right) l \tag{4}$$

where the t_1 and t_2 are the time settings of thermal emission rate window e_T, α is the absorption coefficient dependent on the wavelength (λ) of the light used for the excitation of charge carriers, L_D is

the diffusion length and l is the width of the electrodes. Usually, at least three values of $n_T(0)$ corresponding to various values of e_T are determined and in the second step, the trap concentration is calculated by the extrapolation of the $n_T = f(e_T)$ relationship to the value of $e_T \to 0$ according to the formula:

$$n_T(0) = \frac{N_T}{1 + \frac{e_T}{G\tau c_T}} \tag{5}$$

where the G is the generation rate of electron–hole pairs, τ is the charge carriers lifetime and c_T is the capture coefficient of charge carriers.

The images of the correlation spectral fringes, obtained by the two-dimensional analysis of the temperature dependence of the decay rate of the photocurrent relaxation waveforms recorded for A and B samples at temperatures ranging from 200 to 320 K, are presented in Fig. 7(a) and (b), respectively.

It is easily seen that the broad correlation spectral fringes consist of several overlapping ones related to different defect levels.

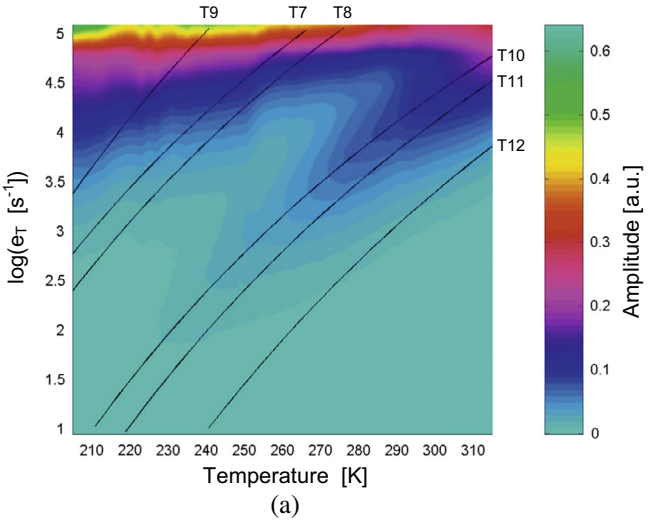

Fig. 7. Images of the correlation spectral fringes obtained by the HRPITS technique for deep-level defects induced in a FZ Si wafer by the irradiation with a high-energy deuteron beam. (a) Fringes for radiation centers in the A sample located on the wafer at a distance of 2 mm from the region irradiated with the maximum deuteron beam intensity. (b) Fringes for radiation centers in the B sample located on the wafer at 10 mm from the region irradiated with the maximum deuteron beam intensity.

The solid lines in these figures illustrate the temperature dependences of the emission rate of charge carriers for detected radiation defect centers and are the signatures of these defects. In the A sample, we have revealed six defect centers with various properties and concentrations labeled as T7, T8 T9, T10, T11, and T12. In the B sample, the radiation defects labeled as T7 and T8 are not observed. However, another defect center, labeled as T13 is formed. This fact indicates that the radiation defect structure of FZ Si is dependent on the deuteron beam intensity. Fig. 8 shows the image of the correlation spectral fringes determined from the photocurrent relaxation waveforms recorded for the C sample in the temperature range of 200–320 K. This image indicates that the folds related to the thermal emission of charge carriers in the 3D HRPITS correlation spectra are very weak. Therefore, it was not possible to resolve for this sample the temperature dependences of emission rate of charge carriers using the 2D ILT procedure. From the amplitude of the relaxation waveforms we have estimated that the concentrations of radiation defect centers in this sample are likely to be by two orders of magnitude lower compared to the concentrations in the A and B samples. It worth noting that the C sample represents the region located in the Si wafer at the distance of 18 mm from the region that have been irradiated with the maximum deuteron intensity. So, this sample has been irradiated with the much smaller deuteron dose than the A and B samples located on the Si wafer at the distance of 2 and 10 mm from the region irradiated with the maximum deuteron beam intensity, respectively.

Thus, our results presented in this paper are in good agreement with the previous results [23] showing that the radiation defect structure of Si is strongly dependent on the fluence of high-energy particles. The solid lines in Fig. 7 illustrate the temperature dependences of emission rate of charge carriers determined from the photocurrent relaxation waveforms by a multi-exponential analysis using the two-dimensional procedure based on the inverse Laplace transform algorithm. The values of the activation energy E_a and factor A in the Arrhenius equation, determined from the temperature dependences of emission rate (solid lines in Fig. 7(a) and (b)), are listed in Table 2. In this table, the estimated concentrations of defect centers (N_T) are also included and the centers tentative identification is given. The results summarized in Table 2 indicate that the radiation defect structure of FZ Si induced by the various

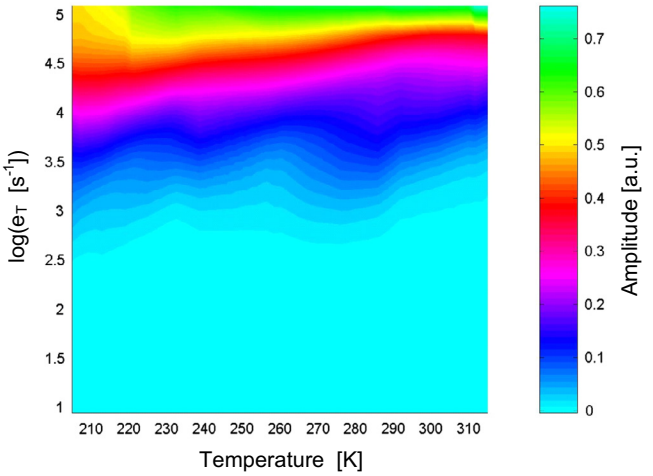

Fig. 8. Image of HRPITS correlation spectrum obtained by the analysis of the photocurrent relaxation waveforms recorded in the temperature range 200–320 K for the C sample located on the FZ Si wafer at 18 mm from the region irradiated with the maximum deuteron beam intensity. Because of the low concentration of deep-defect centers, the weak amplitudes of the relaxations waveforms related to the thermal emission of charge carriers not allow to unambiguously determine the temperature dependences of emission rate.

Table 2
Summary of deep defect centers properties and concentrations for the A and B samples located in the FZ Si wafer at the distance of 2 and 10 mm, respectively, from the region irradiated with the maximum intensity of the 4.4-GeV deuteron beam.

Trap Label	E_a [meV]	A [s^{-1} K^{-2}]	Sample A	Sample B	Tentative identification
			N_T [cm^{-3}]	N_T [cm^{-3}]	
T7	360 ± 15	1.0×10^7	3.2×10^{15}	–	V_3 (2−/−) or C_iO_i (+/0)
T8	380 ± 15	1.3×10^7	2.5×10^{15}	–	V_4 (2−/−)
T9	410 ± 20	1.3×10^9	4.3×10^{15}	1.5×10^{15}	V_2H (−/0)?
T13	420 ± 20	9.6×10^6	–	1.0×10^{15}	V_2 (−/0)
T10	430 ± 20	4.5×10^6	4.0×10^{15}	2.8×10^{15}	V_3 (−/0)
T11	460 ± 20	7.6×10^6	7.8×10^{15}	3.9×10^{15}	V_4 (−/0)
T12	530 ± 20	2.2×10^7	3.5×10^{15}	2.3×10^{15}	V_5 (−/0)

intensity of the 4.4-GeV deuterons is qualitatively and quantitatively different. For the material irradiated with the almost maximum deuteron beam intensity (sample A), we have found six defect centers: T7, T8, T9, T10, T11, and T12 with the activation energies of 360, 380, 410, 430, 460, and 530 meV, respectively. The concentrations of these centers are in the range of 2.5×10^{15}–7.8×10^{15} cm^{-3}. For the material irradiated with a significantly lower intensity of the deuteron beam, five defect centers: T9, T13, T10, T11, and T12 with the activation energies of 410, 420, 430, 460, and 530 meV, respectively, have been found. The concentrations of these centers are in the range of 1.0×10^{15}–3.9×10^{15} cm^{-3}. In view of the results presented in [12,34], the properties of T7 (360 meV) and T10 (430 meV) centers are in very good agreement with those attributed to the trivacancy (V_3). These results show that V_3 that is built up of the chain of single vacancies occurring in (1 1 0) plane gives rise to the two acceptor levels located at a small distance above the midgap.

According to DLTS measurements, the two levels corresponding to the various charge states of trivacancy, namely to V_3 (2−/−) and V_3 (−/0), are located at 0.36 and 0.46 eV below the conduction band edge (E_c), respectively [34]. Moreover, the results of *ab initio* calculation confirm that the first acceptor level of V_3 (−/0) with the C_{2v} symmetry is placed deeper in the bandgap than the second level of V_3 (2−/−) [12,34,35]. Similarly, as it follows from theoretical estimations, the two acceptor levels corresponding to the various charge states of tetravacancy, namely to V_4 (2−/−) and V_4 (−/0), are located slightly deeper in the bangap than those of V_3 (2−/−) and V_3 (−/0) [12,35]. Thus, the T8 (380 meV) and T11 (460 meV) traps are likely to be attributed to the two energy levels related to the various charge states of the tetravacancy. The parameters of the T13 trap are perfectly consistent with those previously determined for the divacancy V_2 (−/0) [23,24].

It should be noted that the electronic properties of divacancy in silicon have been well known for more than decade [23,24,36]. The midgap center with the activation energy of 530 meV can be identified with the I-center produced in FZ silicon by high doses of γ irradiation [23,24]. According to DLTS studies the I center is an electron trap located in the bandgap at E_c – 0.545 eV [25]. So far, the atomic configuration of this center has not been definitively established, however, taking into account the results reported in [12,35,36], this midgap center seems to be related to the pentavacancy V_5 (−/0). The T9 center can be assigned to a hydrogen-related electron trap, located in the bandgap approximately at E_c – 0.43 eV, introduced in FZ silicon by MeV proton implantation [37]. This trap has been tentatively attributed to a complex involving a hydrogen atom and a divacancy (a V_2H complex).

According to the results demonstrated in Table 2, the main deep defect centers induced by the 4.4-GeV deuteron irradiation are tentatively identified with deep acceptors related to vacancy aggregates. However, the parameters of trap T7 are also consistent with the signatures reported for the deep donor center, with the activation energy around 360 meV above the valence band edge, identified with the complex involving interstitial-carbon and interstitial oxygen (C_iO_i (+/0)) [38]. This defect arises as a result of the reaction of a mobile C_i atom with an oxygen interstitial and is among the most dominant centers observed in Si after irradiation with electrons or hadrons at room temperature [39,40]. Being a deep donor, the C_iO_i center may play an important role in the compensation of deep acceptor centers and contribute to the increase in the material resistivity after irradiation.

The concentrations of detected defect centers are significantly dependent on the deuteron beam intensity. The predominant radiation defects in the both A and B samples, located from the region irradiated with the maximum intensity of the 4.4-GeV deuteron beam at the distance of 2 and 10 mm, respectively, are tetravacancies with the activation energy of 460 meV. It is very likely that tetravacancies are formed by the reaction between divacancies: $V_2 + V_2 \rightarrow V_4$ [12,35,36]. The results of HRPITS measurements allow for proposing a mechanism responsible for the increase in the material resistivity from $\sim 2 \times 10^4$ to $\sim 3 \times 10^5$ Ω cm resulting from the deuteron irradiation. It worth noting that the shallow acceptor concentration in the starting *p*-type FZ Si, associated mainly with the residual boron concentration, is very likely to be below of 10^{12} cm^{-3}. In other words, this concentration is much lower than the concentration of deep acceptors formed during the irradiation. Thus, the increase in the material resistivity is primarily associated with the charge compensation of irradiation-induced electrically active defect centers and not with the passivation of the residual shallow acceptors. These defects are likely to be the shallow donors, related to the irradiation-induced oxygen aggregates and the deep acceptor centers, related to the vacancy aggregates. The compensation may be also enhanced by the contribution of deep donors formed by the interstitial-carbon interstitial-oxygen (C_iO_i) pairs.

4. Conclusions

The resistivity map obtained with the SPDR technique enabled us to obtain a permanent fingerprint of the deuteron beam intensity profile. It has been shown that after the 4.4-GeV deuteron irradiation, the resistivity of silicon wafer region irradiated with the maximum beam intensity increases around 15 times with respect to the resistivity before irradiation. The maximum resistivity value of 3.9×10^5 Ω cm is consistent with the resistivity of intrinsic silicon. The results of the capacitance measurements in the frequency domain have shown the presence of depletion layers in the virgin and irradiated wafers, which are related to the presence of surface state charges.

By using the HRPITS technique, we have shown that the irradiation of FZ Si with the 4.4-GeV deuterons results in the formation of seven types of deep-level defects with the activation energies of 360, 380, 410, 420, 430, 460, and 530 meV. The predominant 460-meV defect centers are likely to be attributed to tetravacancies (V_4), whose concentration is significantly dependent on the deuteron dose. The tentative identification of detected centers

indicates that the irradiation-induced increase in the material resistivity may be due to the compensation of shallow donors, related to irradiation-induced oxygen aggregates, with deep acceptors, related to the vacancy aggregates. The compensation may be also enhanced by the contribution of deep donors formed by the interstitial-carbon interstitial-oxygen (C_iO_i) pairs.

Acknowledgement

This research was supported by the Grant of the Polish Plenipotentiary to JINR.

References

[1] J. Janesick, G. Soli, T. Elliot, S. Collins, Proc. SPIE 1447 (1991) 87.
[2] C.J. Bebek, D.E. Groom, S.E. Holland, A. Karcher, W.F. Kolbe, J. Lee, M.E. Levi, N.P. Palaio, B.T. Turko, M.C. Uslenghi, M.T. Wagner, G. Wang, IEEE Trans. Nucl. Sci. 49 (2002) 1221–1225.
[3] P. Hazdra, K. Brand, J. Vobecký, Nucl. Instr. Meth. B 192 (2002) 291.
[4] S.K. Dubey, A.D. Yadav, B.K. Kamalapurkar, T.K. Gundu Rao, M. Gokhale, T. Mohanty, D. Kanjilal, Nucl. Instr. Meth. B 244 (2006) 157.
[5] M. Jadan, A.R. Chelyadinskii, V.Yu. Yavid, Nucl. Instr. Meth. B 225 (2004) 516.
[6] E. Simoen, C. Claeys, V. Privitera, S. Coffa, M. Kokkoris, E. Kossionides, G. Fanourakis, A. Nylandsted Larsen, P. Clauws, Nucl. Instr. Meth. B 186 (2002) 19.
[7] M. Moll, E. Fretwurst, M. Kuhnke, G. Lindstrom, Nucl. Instr. Meth. Phys. Res., B 186 (2002) 100.
[8] M. Kuhnke, E. Fretwurst, G. Lindstroem, Nucl. Instr. Meth. Phys. Res., B 186 (2002) 144.
[9] D. Konozenko, A.K. Semenyuk, W.I. Khivrich, in: I.W. Corbett, G.D. Watkins (Eds.), Conf. Proc. on Radiation Effects in Semiconductors, Gordon and Breach Science Publishers, Albany, 1970.
[10] E. Borchi, M. Bruzzi, B. Dezillie, S. Lazanu, Z. Li, S. Pirollo, IEEE Trans. Nucl. Sci. 46 (1999) 834.
[11] N.T. Bagraev, Semicond. Sci. Technol. 9 (1994) 61.
[12] P.F. Ermolov, D.E. Karmanov, A.K. Leflat, V.M. Manankov, M.M. Merkin, E.K. Shabalina, Semiconductors 36 (2002) 1114.
[13] J. Janesick, Scientific Charge-Coupled Devices, SPIE Press, 2001.
[14] G.D. Watkins, J.W. Corbett, Phys. Rev. 138 (1965) A543.
[15] R.E. Whan, J. Appl. Phys. 37 (1966) 3378.
[16] Young-Hoon Lee, James W. Corbett, Phys. Rev. B 8 (1973) 2810.
[17] D.V. Lang, J. Appl. Phys. 45 (1974) 3023.
[18] G.D. Watkins, J.R. Troxell, Phys. Rev. Lett. 44 (1980) 593.
[19] B.G. Svensson, B. Mohadjeri, Phys. Rev. B 43 (1991) 2292.
[20] E. Simoen, C. Claeys, V. Privitera, S. Coffa, M. Kokkoris, E. Kossionides, G. Fanourakis, A. Nylandsted Larsen, P. Clauws, Nucl. Instr. Meth. Phys. Res., B 186 (2002) 19.
[21] J. Krupka, Meas. Sci. Technol. 24 (2013) 062001.
[22] J. Krupka, J. Judek, T. Ciuk, 17th International Conference on Crystal Growth and Epitaxy, Warsaw, August 11–16, 2013.
[23] R. Kozłowski, P. Kamiński, E. Nossarzewska-Orłowska, E. Fretwurst, G. Lindstroem, M. Pawłowski, Nucl. Instr. Meth. Phys. Res., A 552 (2005) 71.
[24] P. Mangiagalli, M. Levalois, P. Marie, P.G. Rancoita, M. Rattaggi, Eur. Phys. J. Appl. Phys. 6 (1999) 121.
[25] Y. Omura, Y. Zohta, M. Kanazawa, Solid State Commun. 11 (1972) 263.
[26] R. Kozłowski, P. Kamiński, E. Nossarzewska-Orłowska, Nucl. Instr. Meth. Phys. Res., A 476 (2002) 639.
[27] D.J. Chadi, Phys. Rev. B 41 (1990) 10595.
[28] V.V. Voronkov, Semicond. Sci. Technol. 8 (1993) 2037.
[29] A.S. Oates, M.J. Binns, R.C. Newman, J.H. Tucker, J.G. Wilkes, A. Wilkinson, J. Phys. C: Solid State Phys. 17 (1984) 5695.
[30] U. Gösele, T.Y. Tan, Appl. Phys. A 28 (1982) 79.
[31] Keon M. Lee, J.M. Trombetta, G.D. Watkins, Mater. Res. Soc. Symp. Proc. 46 (1985) 263.
[32] J.C. Bourgoin, M. Zazoui, S. Alaya, T. Neffati, J. Phys. Fr. 7 (1997) 2145.
[33] M. Pawłowski, P. Kamiński, R. Kozłowski, S. Jankowski, M. Wierzbowski, Metrol. Meas. Syst. XII (2005) 207.
[34] V.P. Markevich, A.R. Peaker, S.B. Lastovskii, L.I. Murin, J. Coutinho, V.J.B. Torres, P.R. Briddon, L. Dobaczewski, E.V. Monakhov, B.G. Svensson, Phys. Rev. B 80 (2009) 235207.
[35] J.L. Hastings, S.K. Estreicher, P.A. Fedders, Phys. Rev. B 56 (1997) 10215.
[36] G.D. Watkins, Mater. Sci. Semicond. Process. 3 (2000) 227.
[37] P. Lévêque, A. Hallén, B.G. Svensson, J. Wong-Leung, C. Jagadish, V. Privitera, Eur. Phys. J. Appl. Phys. 23 (2003) 5.
[38] M. Yamaguchi, A. Khan, S.J. Taylor, K. Ando, T. Yamaguchi, S. Matsuda, T. Aburaya, J. Appl. Phys. 86 (1999) 217.
[39] P. Kaminski, R. Kozlowski, A. Jelenski, T. Mchedlidze, T. Suezawa, Jpn. J. Appl. Phys. 42 (2003) 5415.
[40] V. Eremin, A. Ivanov, E. Verbitskaya, Z. Li, S.U. Pandey, Nucl. Instr. Meth. Phys. Res., A 426 (1999) 120.